

Precession Interpretation of the Isolated Pulsar PSR B1828-11

Bennett Link¹

*Montana State University, Department of Physics, Bozeman MT 59717;
blink@dante.physics.montana.edu*

and

Richard I. Epstein

*Los Alamos National Laboratory, Mail Stop D436, Los Alamos, NM 87545;
epstein@lanl.gov*

ABSTRACT

Pulse timing of the isolated pulsar PSR B1828-11 shows strong Fourier power at periods $\simeq 1000$, 500 and 250 d, correlated with changes in the pulse profile (Stairs, Lyne & Shemar 2000). We study the extent to which these data can be explained by precession of the star's rigid crust coupled to the magnetic dipole torque. We find that the correlated changes in the pulse duration and spin period derivative can be explained as precession at a period of $\simeq 500$ d with a wobble angle of $\simeq 3^\circ$ if the star's dipole moment is nearly orthogonal to its symmetry axis. The dipole torque produces a harmonic at ~ 250 d. Comparison of the predicted spin dynamics with the observed pulse durations requires the radio beam to have a non-standard "hour-glass" shape. We make predictions of variations in beam polarization and pulse profile with which to test this interpretation. The precession interpretation of PSR B1828-11 seriously challenges the current understanding of the liquid interior of the neutron star. In particular, if the internal liquid is in a superfluid state, its rotational vortices cannot be significantly pinned to the crust.

Subject headings: dense matter — magnetic fields — stars: magnetic fields — stars: neutron — pulsars: individual (PSR B1828-11)

¹Also Los Alamos National Laboratory

Table 1: Spin Parameters of PSR B1828-11^a

period p	0.405 s
\dot{p}	$60.0 \times 10^{-15} \text{ s s}^{-1}$
Spindown age $t_{\text{age}} \equiv p/2\dot{p}$	0.11 Myr

^aStairs, Lyne & Shemar 2000

1. Introduction

The monitoring of pulsar spin behavior through precision timing measurements provides a means for studying the dynamics and internal structure of neutron stars. In this connection, detection of precession in pulsars is of particular interest. Relativistic (geodesic) precession has been observed in the double neutron star binaries PSRs B1913+16 and B1534+12 (Weisberg, Romani & Taylor 1989; Arzoumanian 1995), and provides confirmation of General Relativistic orbital mechanics. Classical precession in isolated pulsars could probe the coupling of the stellar crust to the interior, but its detection is complicated by the presence of timing noise. Evidence for long-period precession is seen in the Crab pulsar (Lyne, Pritchard & Smith 1988), the Vela pulsar (Deshpande & McCulloch 1996) and PSR B1642-03 (Cordes 1993; Shabanova, Lyne & Urama 2001). The 35-d periodicity seen in the accreting system Her X-1 (Tannanbaum *et al.* 1972) has been interpreted as precession by many authors (*e.g.*, Brecher 1972; Trümper *et al.* 1986; Cadez, Galicic & Calvani, 1997; Shakura, Postnov & Prokhorov 1998).

Recently, Stairs, Lyne & Shemar (2000) discovered the most compelling evidence to date for precession of an isolated neutron star. The period residuals of PSR B1828-11 have an amplitude of ~ 1 ns and have strong Fourier power at periods of $\simeq 1000$ d, 500 d and 250 d. These Fourier components alone might suggest a Doppler effect through gravitational interaction with planets. However, correlations of the pulse shape and duration with variations in the period derivative \dot{p} strongly suggest that the viewing angle with respect to the emission beam is varying, as one would expect if the star were precessing (see Fig. 1). There is no obvious damping of the observed fluctuations, though the timing behavior is not entirely stable. See Table 1 for the spin parameters of PSR B1828-11.

The purpose of this paper is to investigate if the timing behavior and pulse profile changes of PSR B1828-11 can be quantitatively understood in terms of stellar precession. We assume that the observed timing residuals represent true changes in the pulsar’s rotation rate. An immediate question is which of the three observed Fourier components corresponds

to the actual precession frequency. The residuals of the period p and period derivative \dot{p} show the strongest Fourier power at $\simeq 500$ d (see Fig. 1 and Stairs, Lyne & Shemar 2000 Fig. 3); we tentatively assume that this Fourier component represents the precession period. The *wobble angle* θ between the star’s symmetry axis and its angular momentum can be estimated from the pulse profile changes. The difference in widths between the “wide” and “narrow” beam profiles is $\simeq 2^\circ$ (see Fig. 2), implying a wobble angle of similar magnitude for plausible beam shapes.

This precession interpretation could be complicated by magnetospheric processes. Precession of the star could create changes in the magnetosphere that affect the geometry and location of the emission region. Changes in the height of the emission region would introduce light-travel time contributions to the pulse arrival times. Different regions of the magnetosphere might be viewed as the star precesses. We do not consider these effects in this paper.

In the next section, we give an overview of precession. In §3 we study how the electromagnetic torque, responsible for the star’s spin down (at least in part), modifies precession. In §4, we relate this torque effect to the observed timing. In §5, we propose a model of the the observed pulse duration variations. In §6 we discuss some of our chief results. We conclude with discussion of observational tests of the precession interpretation.

2. Overview

Most treatments of pulsar precession to date have considered mainly *free* precession (*e.g.*, Goldreich 1970; Pines & Shaham 1974; Shaham 1977; Suto & Iso 1985; Orford 1987; Bisnovatyi-Kogan, Mersov & Sheffer 1989; Glendenning 1990; Nelson, Finn & Wasserman 1990; Bisnovatyi-Kogan & Kahabka 1993; Cadez, Galicic & Calvani 1997; Shakura, Postnov & Prokhorov 1998; Sedrakian, Wasserman & Cordes 1999; Jones & Andersson 2000). The observed variations in p and \dot{p} in PSR B1828-11, however, are far too large to be explained by free precession for a wobble angle of $\theta \sim 2^\circ$. In §3 we calculate the precession of a neutron star subject to a vacuum magnetic dipole braking torque and find a solution that is consistent with observations.

Consider first the free precession of a biaxial neutron star; the geometry is as shown in Fig. 3. At any instant, the symmetry axis \hat{e}_3 , angular momentum \mathbf{L} and angular velocity $\boldsymbol{\omega}$ span a plane. Let the oblateness be $\epsilon \equiv (I_3 - I_1)/I_1$, where I_3 and I_1 are the largest and smallest moments of inertia about the principal axes. For small oblateness $\epsilon \ll 1$, the angle between \mathbf{L} and $\boldsymbol{\omega}$ is $\hat{\theta} \simeq \epsilon\theta \ll \theta$ (see, *e.g.*, Jones & Andersson 2000). In the inertial frame, \hat{e}_3

and $\boldsymbol{\omega}$ rotate in a right-handed sense about \mathbf{L} at frequency $\simeq \omega(1 + \epsilon)$. Combined with this motion is a slow *retrograde* motion of the body about \hat{e}_3 at precession frequency $\omega_p \simeq \epsilon\omega$.

For a precessing pulsar, the pulse emission times are defined by the instants at which the beam center passes closest to the direction of the observer; the observed arrival times are simply offset from the emission times (apart from Doppler shifts from translational motion). If the star is freely precessing, the pulse arrival times vary sinusoidally as $\Delta t \simeq (p_0/2\pi)\theta \cot \chi \sin(\omega_p t + \beta)$ where p_0 is the spin period, $\chi > \theta$ is the inclination angle between the center of the pulsar beam and the body’s symmetry axis and β is a phase (see Nelson, Finn & Wasserman 1990). This variation is a purely geometrical effect, as the magnitude of the angular velocity is unchanged by free precession. The corresponding changes in period derivative due to this geometrical effect are $\Delta \dot{p} \simeq (2\pi)^{-1}(p_0\omega_p)^2\theta \cot \chi \sin(\omega_p t + \beta)$ (see eq. 21 below). For a precession period of 500 d and $\chi > 30^\circ$, the residuals in \dot{p} are less than 0.02 s s^{-1} , a factor of at least 10 smaller than observed.

The electromagnetic torque on a neutron star modifies the precession and increases the magnitude of timing residuals for a given wobble angle (Jones 1988; Cordes 1993; Jones & Andersson 2000). In the body frame of a precessing object, the angular velocity vector $\boldsymbol{\omega}$ moves about the body’s symmetry axis \hat{e}_3 at frequency ω_p in a right-handed sense. For a magnetized neutron star with a magnetic moment misaligned with respect to the symmetry axis, the angle between the dipole moment \mathbf{m} and $\boldsymbol{\omega}$ changes by about θ over a precession period (see eq. 22 below). The external dipole torque, which depends on this angle, thus varies over a *precession* period in addition to its slow decay over an evolutionary timescale. For small wobble angle θ , these torque changes produce changes in the star’s spin rate ω of (see eq. 13)

$$\frac{\Delta\dot{\omega}}{\omega_0} = \frac{\theta}{2\tau} \left[\sin 2\chi \cos(\omega_p t + \beta) + \frac{\theta}{2} \sin^2 \chi \cos(2\omega_p t + 2\beta) \right], \quad (1)$$

For simplicity we assume that the pulsed radiation is emitted along the axis of the magnetic dipole, *i.e.*, both the beam and the dipole are at an angle χ with respect to the body’s symmetry axis. The torque-induced timing variations are much larger than the geometrical effects associated free precession (Cordes 1993; Jones 1988; see eq. 21 below). In addition, and as pointed out by Jones & Andersson (2000), the dependence of the torque on the angle between the star’s angular velocity and its dipole moment creates a strong harmonic of the precession frequency in the star’s spin rate *if the star is a nearly orthogonal rotator*. In §5 we apply this picture to PSR B1828-11 and find that $\chi = 89^\circ$ and a wobble angle of $\theta \simeq 3^\circ$ can account for the 500-d Fourier component with a harmonic at 250 d. Precession does not give the whole story, however, as it does not explain the Fourier power at 1000 d.

As the star precesses we see different sweeps through the beam of the pulsar, allowing

us to partially map the beam morphology. As we will show, the observed variations in pulse duration imply that the beam has an “hour glass” shape, *i.e.*, the pulse duration is longer for sweeps farthest from the beam center.

3. Precession Under the Dipole Torque

Precession of a neutron star will occur if the symmetry axis of the crust is not aligned with the angular momentum. The elastic crust has two contributions to its oblateness: a *centrifugal deformation* associated with the star’s spin and a *Coulomb deformation* sustained by the rigidity of the lattice (Alpar & Pines 1985; Jones & Andersson 2000). The principal axis of inertia of the centrifugal deformation follows the instantaneous spin axis of the crust, and so does not affect the precession. In §6 we discuss possible origins of Coulomb deformation.

The period and amplitude of the crust’s precession are affected by the coupling of the crust to the liquid interior. The precession creates time-dependent velocity differences between the crust and liquid that vary over the star’s spin period. If the coupling time τ_f between the crust and the liquid interior is much longer than the crust’s spin period p , the precession will damp over $\simeq 2\pi\tau_f/p$ precession periods (Bondi & Gold 1955; Sedrakian, Wasserman & Cordes 1999). All studies of damping of differential rotation between the crust and various parts of the liquid interior give $\tau_f \gg p$ (*e.g.*, Alpar & Sauls 1988; Epstein & Baym 1992; Jones 1992; Abney, Epstein & Olinto 1996; Mendell 1998). To a good approximation, therefore, the liquid interior can be treated as *decoupled* from the solid (Bondi & Gold 1955; Sedrakian, Wasserman & Cordes 1999); in this regime the crust precesses almost as if the liquid interior were not there.²

In our calculations we treat the neutron star as consisting of a biaxial, rigid crust afloat on a liquid core. The solid portion of the star comprises less than 1% of the star’s total moment of inertia and we regard the liquid of the inner crust as an extension of the core liquid. We neglect angular momentum exchange between the solid and the liquid. For simplicity we ignore the centrifugal bulge (which does not affect the precession) and treat the crust as perfectly rigid. For illustration we describe the spin dynamics of the crust with

²A precessing rigid shell containing a non-spherical normal fluid is *inertially coupled* to the fluid (Lamb 1952). The fluid, which tends to a configuration symmetric about its rotation axis, exerts a reaction force on the solid. The relevance of this effect to an elastic neutron star containing superfluid neutrons and protons is unclear. Inertial coupling would not change the precession dynamics that we calculate in this paper, though it would change the dependence of the precession period on the crust oblateness.

the vacuum dipole torque of Davis & Goldstein (1970). While plasma effects could contribute to the spin down, a torque similar to the vacuum torque will always be present. In a frame corotating with the crust, the equations of motion are (Goldreich 1970; Melatos 2000)

$$\mathbf{I} \cdot \frac{d\boldsymbol{\omega}}{dt} + \boldsymbol{\omega} \times \mathbf{L} = \frac{2\omega^2}{3c^3}(\boldsymbol{\omega} \times \mathbf{m}) \times \mathbf{m} + \frac{1}{Rc^2}(\boldsymbol{\omega} \cdot \mathbf{m})(\boldsymbol{\omega} \times \mathbf{m}), \quad (2)$$

where \mathbf{I} is the moment of inertia tensor of the crust, $\boldsymbol{\omega}$ is the angular velocity, \mathbf{L} is the angular momentum, \mathbf{m} is the magnetic dipole moment (centered on the star) and R is the radius of the star. The first contribution to the torque is due to the radiation far field and is responsible for spinning down the star. The second term represents the near-field radiation torque. The coefficient of this term depends on how the star's internal magnetization is treated (Melatos 2000); its precise value does not affect our results. We will find that variations in the spin rate associated with precession are determined predominantly by the far-field torque (see. eq. 13).

We define a Cartesian coordinate system (1,2,3) with the 3 axis along the symmetry axis \hat{e}_3 of the crust. Without loss of generality, we take the magnetic dipole to lie in the 1-3 plane, inclined with respect to the 3 axis by an angle $\chi < \pi/2$. At $t = 0$ the spin rate is $\omega_0 \equiv 2\pi/p_0$. The equations of motion are

$$I_1\dot{\omega}_1 + \omega_2\omega_3(I_3 - I_1) = T_1 = \frac{1}{2\tau}I_3(\omega_3 \sin \chi - \omega_1 \cos \chi) \cos \chi + \frac{3x_0^{-1}}{4\tau}I_3(\omega_1 \sin \chi + \omega_3 \cos \chi)\omega_2 \sin \chi \quad (3)$$

$$I_1\dot{\omega}_2 - \omega_1\omega_3(I_3 - I_1) = T_2 = -\frac{1}{2\tau}I_3\omega_2 + \frac{3x_0^{-1}}{4\tau}I_3(\omega_1 \sin \chi + \omega_3 \cos \chi)(\omega_3 \sin \chi - \omega_1 \cos \chi) \quad (4)$$

$$I_3\dot{\omega}_3 = T_3 = \frac{1}{2\tau}I_3 \sin \chi(\omega_1 \cos \chi - \omega_3 \sin \chi) - \frac{3x_0^{-1}}{4\tau}I_3(\omega_1 \sin \chi + \omega_3 \cos \chi)\omega_2 \sin \chi, \quad (5)$$

where $\tau \equiv 3c^3 I_3 / 4m^2 \omega_0^2$ is the characteristic time over which the far-field torque spins down the star, $m \equiv |\mathbf{m}|$ and $x_0 \equiv R\omega_0/c \ll 1$. For the oblate star, $I_3 > I_2 = I_1$. Terms on the right-hand side of eqs. [3]-[5] proportional to x_0^{-1} arise from the near-field torque; the remaining terms are due to the far-field torque. The near-field torque is stronger than the far-field torque by a factor $\simeq x_0^{-1}$, though its direction is always orthogonal to $\boldsymbol{\omega}$.

Identification of the small parameters in the problem allows perturbative treatment of the torque. Because the torque acts over timescales that are much longer than the observed precession period, we expect the spin solution to resemble that for free precession. Hence,

the ratio ω_p/ω_0 , where ω_p is the frequency of free precession, should be approximately $\epsilon \equiv (I_3 - I_1)/I_1$. This ratio is $\simeq 10^{-8}$ for PSR B1828-11 if the precession period is $\simeq 500$ d. Changes in the pulse duration (Fig. 2) through the precession period suggest a wobble angle of $\theta \sim 2^\circ$. For these small values of ϵ and θ , $\hat{\theta} \simeq \epsilon\theta \ll \theta$, so θ and α are nearly equal (Jones & Andersson 2000). In terms of the components of the angular velocity, α is approximately $(\omega_1^2 + \omega_2^2)^{1/2}/\omega_0 \ll 1$. We therefore regard ω_1 and ω_2 as perturbations about the secular spin down. The relative magnitudes of the small dimensionless parameters are given by

$$1 \gg \alpha \gg \epsilon \gg \epsilon\alpha > x_0^{-1} \frac{1}{\omega_0\tau} \gg \frac{1}{\omega_0\tau}. \quad (6)$$

To order $\epsilon\omega_1$ and $\epsilon\omega_2$, eqs. [3] and [4] are

$$\dot{\omega}_1 + \epsilon\omega_2\omega_0 = 0 \quad (7)$$

$$\dot{\omega}_2 - \epsilon\omega_1\omega_0 = 0. \quad (8)$$

For $\alpha \ll 1$, the solutions are

$$\omega_1 = \omega_0\alpha \cos(\omega_p t + \beta) \quad (9)$$

$$\omega_2 = \omega_0\alpha \sin(\omega_p t + \beta) \quad (10)$$

$$\omega_p = \epsilon\omega_0 = \frac{I_3 - I_1}{I_1}\omega_0, \quad (11)$$

where β is a phase. The behavior of the component of the angular velocity orthogonal to the symmetry axis is essentially unaltered by the torque; the precession frequency is that of free precession and $\alpha \simeq \sin \alpha = (\omega_1^2 + \omega_2^2)^{1/2}/\omega_0 = \text{constant}$. In the body frame, both \mathbf{L} and $\boldsymbol{\omega}$ (which are always coplanar with \hat{e}_3) precess slowly at frequency $\omega_p \ll \omega_0$ about \hat{e}_3 and in the same sense. For the limit $\epsilon \ll 1$ that we are considering, α and θ are nearly equal.

For biaxial free precession, $\omega \equiv |\boldsymbol{\omega}|$ is constant. Under the dipole torque, however, ω undergoes changes that are important for the observed timing behavior. Combining eqs. [3]-[5] gives

$$\frac{d\omega^2}{dt} = \frac{2}{I_1} \left(\boldsymbol{\omega} \cdot \mathbf{T} - \epsilon \frac{I_1}{I_3} \omega_3 T_3 \right). \quad (12)$$

The $\boldsymbol{\omega} \cdot \mathbf{T}$ term does not depend on the near-field torque. The near-field torque changes the spin rate only through the small final term, which we will neglect. The secular spindown in the absence of precession is given by $\dot{\omega} \simeq -\omega \sin^2 \chi / 2\tau$. Combining eq. [12] with eqs. [9]-[11], setting $\alpha = \theta$, retaining terms to order $\theta^2(\omega_0\tau)^{-1}$, and subtracting the secular spindown gives (dropping constant terms):

$$\frac{\Delta\dot{\omega}}{\omega_0} = \frac{\theta}{2\tau} \left[\sin 2\chi \cos(\omega_p t + \beta) + \frac{\theta}{2} \sin^2 \chi \cos(2\omega_p t + 2\beta) \right]. \quad (13)$$

Hence $\dot{\omega}$ undergoes small variations of order $\theta(\omega_0\tau)^{-1}$ and $\theta^2(\omega_0\tau)^{-1}$, driven by changes in the far-field dipole torque. These torque variations are due to changes in the angle between $\boldsymbol{\omega}$ and \mathbf{m} as $\boldsymbol{\omega}$ precesses through the body. The harmonic at twice the precession frequency arises from quadratic dependences of $\omega_1 T_1$ and $\omega_2 T_2$ on the components of the angular velocity; the harmonic dominates the fundamental for $\theta \tan \chi > 4$. For a small θ , the dipole moment must be nearly orthogonal to the rotation axis for the harmonic to be significant. The small oscillations of $\dot{\omega}$ largely determine the observed pulse timing; they give period variations $\Delta p \simeq -(p_0^2/2\pi)\Delta\dot{\omega}$.

4. Timing

The observed pulse timing at a given time in the precession cycle depends on the star's spin rate and the orientation of the angular velocity $\boldsymbol{\omega}$ with respect to the observer. To relate the solution of the previous section to the observed pulse timing, we go to an inertial coordinate system x, y, z with the angular momentum along the z axis and the observer in the $x - z$ plane with $x > 0$ and $z > 0$. The azimuthal and polar angles of the magnetic dipole \mathbf{m} , Φ and Θ , are given in this frame by

$$\tan \Phi = \frac{m_y}{m_x} = \frac{(\cos \psi \sin \phi + \cos \theta \cos \phi \sin \psi) \sin \chi - \sin \theta \cos \phi \cos \chi}{(\cos \psi \cos \phi - \cos \theta \sin \phi \sin \psi) \sin \chi + \sin \theta \sin \phi \cos \chi} \quad (14)$$

$$\cos \Theta = \frac{m_z}{m} = \sin \theta \sin \psi \sin \chi + \cos \theta \cos \chi, \quad (15)$$

where ψ , the wobble angle θ and ϕ are Euler angles following the definitions of Landau & Lifshitz (1976) and Goldstein (1980).

The pulsar beam is not necessarily in the same direction as the dipole moment. Nevertheless, for simplicity we define a pulse as occurring when the azimuthal angle Φ of the magnetic dipole equals the azimuth of the observer, *i.e.*, when $m_y = 0$ and $\Phi = 0$. Hence $\dot{\Phi}$ is the observed pulse frequency. For small $\theta < \chi$ and $\theta \cot \chi \ll 1$, eqs. [14] and [15] give to second order in θ ,

$$\dot{\Phi} = \dot{\phi} + \dot{\psi} + \theta \cot \chi \dot{\psi} \sin \psi - \frac{\theta^2}{2}(1 + 2 \cot^2 \chi)(2 \cos^2 \psi - 1)\dot{\psi}. \quad (16)$$

The angles ψ and ϕ are given by

$$\psi = \tan^{-1} \frac{L_1}{L_2} = \tan^{-1} \frac{\omega_1}{\omega_2} = \frac{\pi}{2} - \omega_p t - \beta \quad (17)$$

$$\dot{\phi} = \frac{\omega_3 - \dot{\psi}}{\cos \theta} \simeq \omega + \omega_p + \frac{1}{2}\theta^2\omega_p, \quad (18)$$

$$(19)$$

The observed beam sweep rate is (dropping constant terms)

$$\dot{\Phi} = \omega - \theta \omega_p \cot \chi \cos(\omega_p t + \beta) - \theta^2 \omega_p (1 + 2 \cot^2 \chi) \cos^2(\omega_p t + \beta) \quad (20)$$

Hence, the sweep rate is the spin rate plus a modulation at the free precession frequency and its first harmonic. This modulation is a geometrical effect due to variations in the rate at which the beam sweeps past the observer as the symmetry axis precesses about the angular momentum; it is the only modulation that occurs if the precession is free. The sweep rate also changes as ω changes through secular spin-down and the variations $\Delta\omega$ associated with torque variations as the star precesses. We henceforth focus on behavior of the period derivative since, as we will show, the torque changes evaluated in the previous section largely determine the observe spin behavior. Differentiating eq. [20] in time and combining with eqs. [13], [17] and [19], gives the period derivative residuals with respect to the secular spin down:

$$\begin{aligned} \Delta\dot{p} \simeq -\frac{p_0^2}{2\pi} \ddot{\Phi} \simeq & -\frac{p_0}{t_{\text{age}}}\theta \left[\cot \chi \cos(\omega_p t + \beta) + \frac{\theta}{4}\chi \cos(2\omega_p t + 2\beta) \right] \\ & - \frac{1}{2\pi}(p_0\omega_p)^2\theta \left[\cot \chi \sin(\omega_p t + \beta) + \theta(1 + 2 \cot^2 \chi) \sin(2\omega_p t + 2\beta) \right]. \end{aligned} \quad (21)$$

Here $t_{\text{age}} \equiv \tau/\sin^2 \chi$ is the characteristic spin-down age. This equation gives the complete expression for the star’s residuals in \dot{p} . The first set of square brackets gives the residuals due to torque variations from eq. [13]. The second set of square brackets gives the residuals due to geometrical effects (see Nelson, Finn & Wasserman 1990; Jones & Andersson 2000). For PSR B1828-11, the first-order torque effects always dominate the geometrical effects by a factor of ~ 250 if the precession period is $\simeq 500$ d. For the harmonic at frequency $2\omega_p$ to play a role in the timing (terms proportional to θ^2), χ must be nearly $\pi/2$. The near-field torque, because it does not significantly change ω , is unimportant for the small- θ precession that appears to be taking place in PSR B1828-11.

We model the data for the 2000-day span beginning at MJD 49,000 as the observations were most closely spaced during this period and these data show the observed periodicities most clearly. Fitting eq. [21] to the data, neglecting the small geometrical terms, gives the parameters θ , ω_p , β and χ featured in Table 2. Comparison of the fit to the data is shown in Fig. 1.

5. Pulse Duration Variations

The duration of PSR B1828-11’s pulses is seen to change with the same periodic structure as the spin residuals, suggesting different sweeps through the beam as the star precesses.

Table 2: Model Parameters

θ	3.2°
χ	89°
$2\pi/\omega_p$	511 d
ξ	-0.3°

To study this further, consider the behavior of the polar angle Θ of the beam with respect to \mathbf{L} (eq. 15). Expanding eq. [15] to first order in θ , using eq. [17], gives

$$\Theta = \chi - \theta \cos(\omega_p t + \beta). \quad (22)$$

As the star precesses, Θ varies sinusoidally about χ . The variations in the polar angle are in phase with the dominant contribution to the torque variations (the first term in eq. [21]).

To quantify this further, suppose the constant angle between the observer and the angular momentum is $\gamma \equiv \xi + \chi$ (see Fig. 4). We define the *sweep angle* $\Delta\Theta$ as the difference in polar angle between the observer and the dipole at the time of the pulse: $\Delta\Theta = \xi + \theta \cos(\omega_p t + \beta)$. As a simple model of the variations in pulse duration, we suppose that the pulse duration w is a function of $\Delta\Theta$ only. We assume that w has an extremum (it will turn out to be a minimum) for $\Delta\Theta = 0$, corresponding to a viewing angle co-linear with the dipole axis. We take the expansion

$$w = w_0 + w_2(\Delta\Theta)^2. \quad (23)$$

Consistent with Stairs, Lyne & Shemar (2000), we define a *shape parameter* S as

$$w \equiv \max(w)S + \min(w)(1 - S), \quad (24)$$

where $\max(w)$ and $\min(w)$ are the maximum and minimum values of the beam duration in the precession cycle. Combining eqs. [22] and [23] gives

$$S = \begin{cases} 1 - \left(\frac{\Delta\Theta}{|\xi| + \theta}\right)^2 & w_2 > 0 \\ \left(\frac{\Delta\Theta}{|\xi| + \theta}\right)^2 & w_2 < 0. \end{cases} \quad (25)$$

This shape parameter depends on ξ , θ , ω_p , β , and the sign of w_2 but not its magnitude.

With θ , ω_p and β given by the fit to the timing data, the shape parameter is determined entirely by ξ and the sign of w_2 . Interestingly, we find that w_2 must be positive, *i.e.*, the

beam duration is larger for beam sweeps farthest from the dipole axis. Such a beam pattern is not standard, but is *required* by the precession interpretation of PSR B1828-11. The best-fit value of ξ is -0.3° , as given in Table 2. Comparison of the fit to the data is shown in Fig. 1.

6. Discussion

We find an acceptable fit to the data with $\chi = 89^\circ$ between the magnetic dipole and the star’s symmetry axis, a precession period of 511 d and a wobble angle $\theta = 3.2^\circ$. The predicted shape changes are in qualitative agreement with the observations if the angle between the observer and the angular momentum is 88.7° and the radio beam pattern has the “hourglass” shape sketched in Fig. 5. The beam shape that we have inferred differs from the usual picture of a roughly circular pulsar beam, but might be explainable in terms of a patchy beam of the type found by Han & Manchester (2000) in their statistical study of pulsar beam morphology. If the emission is beamed both parallel and anti-parallel to the dipole axis, an inner pulse would be expected for the nearly-orthogonal inclination that we have inferred. None is seen, so the emission pattern must be more complex.

Our model does not account for 1000-d Fourier component seen in the data. However, significant aperiodic variations in the timing seen over timescales of years indicate that more than just precession is at work in PSR B1828-11. Slow changes in the emission region could be a contributing factor. Perturbations to the star’s figure brought about by relaxation of the star’s structure as it spins down could also play a role. Such starquakes would excite precession by perturbing the star’s angular velocity with respect to the symmetry axis (Link, Franco & Epstein 1998). The perturbations would introduce irregular contributions to the magnitude of the wobble angle and the precessional phase (Jones 1988).

Andersson & Jones (2000) have suggested that the 1000-d Fourier component represents the precession period, and that near orthogonality of the dipole moment with respect to the symmetry axis gives a harmonic at 500 d in the spin residuals. This scenario is unlikely for several reasons: 1) near perfect orthogonality ($\chi \gtrsim 89.9^\circ$) is required to keep the first-order torque term in eq. [21] from giving too large a contribution to \dot{p} , 2) the strong Fourier component at 250 d is not accounted for, and, 3) the shape parameter, which would now be periodic at 1000 and 500 d, would bear little resemblance to the data.

The stellar oblateness inferred from the precession period of 511 d is $\epsilon = (I_3 - I_1)/I_1 = 9 \times 10^{-9}$. For comparison, we estimate the maximum Coulomb oblateness. The maximum mass M_m of a “mountain” that the rigid neutron star crust can support is given roughly

by $M_m g \sim B\theta_c/R$ where g is the gravitational acceleration at the stellar surface, B is the bulk modulus of the crust ($\simeq 10^{48}$ erg) and θ_c is the critical strain angle at which the crust fractures. The maximum oblateness sustainable by crust rigidity is thus (see also Ushomirsky, Cutler & Bildsten 2000)

$$\epsilon \equiv \frac{I_3 - I_1}{I_1} \simeq \frac{M_m}{M_c} \sim 10^{-5} \frac{\theta_c}{10^{-2}}, \quad (26)$$

where M_c is the mass of the crust. A mountain could form as the result of a starquake that perturbs the star's principal axis of inertia away from its angular momentum axis (Link, Franco & Epstein 1998). However, even if the crust is relaxed (*i.e.*, unstrained) before it is set into precession, rigidity prevents a portion of the star's bulge from following the instantaneous rotation axis. The effective oblateness due to rigidity is in this case $\epsilon_r \simeq 10^{-5}\epsilon_\Omega$, where ϵ_Ω is the centrifugal oblateness (Alpar & Pines 1985; see also Munk & MacDonald 1960). For PSR B1828-11's spin period $\epsilon_r \simeq 2 \times 10^{-11}(p/0.4 \text{ s})^{-2}$, giving a precession period of 700 yr. We conclude that PSR B1828-11's crust is strained to the extent that the Coulomb oblateness is $\simeq 100$ times larger than ϵ_r . A significantly strained crust can precess at a much higher frequency than the unstrained crust considered in some previous studies (*e.g.*, Goldreich 1970 and Melatos 2000).

The precession of PSR B1828-11 seriously challenges the notion that superfluid vortices of the crust pin to nuclei (*e.g.*, Anderson & Itoh 1975). Pinning would drastically alter the way in which the star precesses. Shaham (1977) showed that very effective pinning changes the precession period to $(I_1/I_p)p$, where I_p is the portion of the star's fluid moment of inertia that is pinned and I_1 is the moment of inertia of the part of the star that is precessing. Sedrakian, Wasserman & Cordes (1999) have shown that Shaham's conclusion is essentially unaltered if the pinning is imperfect. Pulsar glitches, which might arise from variable coupling between the superfluid and the crust, indicate that $I_p/I_{\text{star}} > 1.4\%$ in stars that frequently glitch (Link, Epstein & Lattimer 1999); I_{star} is the total moment of inertia of the star. This degree of pinning in PSR B1828-11 would give a precession period of $\ll 40$ s, far shorter than the observed of 500 d precession period. It may be that vortex pinning is inhibited in stars that undergo precession with amplitudes as large as those in PSR B1828-11.

7. Observational Tests

Our proposed model for the fluctuations in the timing residuals of PSR B1828-11 implies that the pulsed emission should have several specific attributes that may be observationally tested. Fig. 5 illustrates these features that are characteristic of our model. During the 511 day precession cycle the observer sees both the broad upper and lower parts of the beam. One important test of our model would be evidence of these two different parts of

the emission region.

We modeled the observed pulse durations with the parabolic form of eq. (23), giving the overall beam shape illustrated by the dashed lines in Fig. 5. The actual shape of the emission must be more complex, however, as we suggest with the irregular brightness contours also shown in the figure. Additionally, the linear polarization of the emission region is unlikely to be the same in the upper and lower portions of the emission region, as indicated by the double-headed arrows in the figure.

To indicate the possible signatures one may observe, we have marked certain viewing angles (A-C) in Fig. 5 and the corresponding observing times in Fig. 1. The dotted horizontal line in Fig. 5 is the shape equator (perpendicular to the largest principal moment). The horizontal dotted lines A and C give the range of the viewing angles seen from Earth. Line B represents the viewing angle at which the pulse profile is the narrowest. The pulse profile is wider at viewing angle A and widest at viewing angle C.

While the shape parameter is the same at phases above and below phase B, the precise pulse profiles and radio polarization should be noticeably different at these phases. The polarization angle will vary across the emission region so that the polarization direction will change continuously from phase A to C and then reverse going from C to A. Detection of these changes in pulse shape and polarization would indicate that the radio beam has the hour-glass shape we have inferred, and would support the interpretation that PSR B1828-11 is a precessing neutron star.

We thank A. G. Lyne, D. I. Jones, R. Bandiera, A. Melatos, J. Cordes, D. Chernoff and the other participants of the ITP workshop on *Spin and Magnetism in Young Neutron Stars* for helpful discussions. We are grateful to I. Stairs and A. G. Lyne for providing us with the timing data and beam templates for PSR B1828-11. The work was performed under the auspices of the U.S. Department of Energy, and was supported by NASA ATP grant NAG 53688, by IGPP at LANL and in part by the National Science Foundation under Grant No. PHY94-07194.

REFERENCES

- Abney, M., Epstein, R. I. & Olinto, A. V. 1996, ApJ, 466, L91.
- Alpar, M. A. & Pines, D. 1985, Nature, 314, 334.
- Alpar, M. A. & Sauls, J. A. 1988, ApJ, 327, 723.
- Anderson, P. W. & Itoh, N. 1975, Nature, 256, 25.
- Arzoumanian, Z. 1995, Ph. D Thesis, Princeton University.
- Bisnovatyi-Kogan, G. S. & Kahabka, P. 1993, A&A, 267, L43.
- Bisnovatyi-Kogan, G. S., Mersov, G. A. & Sheffer, E. K. 1989, A&A, 221, L7.
- Bondi, H. & Gold, T. 1955, MNRAS, 115, 41.
- Brecher, K. 1972, Nature, 239, 325.
- Cadez, A., Galicic, M. & Calvani, M. 1997; A&A, 324, 1005
- Cordes, J. 1993, in *Planets Around Pulsars*, ASP Conference Series, Vol. 36, pp. 43-60 (Ed: Phillips, Thorsett & Kulkarni).
- Davis, L. & Goldstein, M. 1970, ApJ, 159, L81.
- Desphande, A. A. & McCulloch, P. M. 1996, in ASP Conference Series, Vol. 105, p. 101 (Ed: Johnston, Walker & Bailes).
- Epstein, R. I. & Baym, G. 1992, ApJ, 387, 276.
- Glendenning, N. K. 1990, ApJ, 359, 186.
- Goldreich, P. 1970, ApJ, 160, L11.
- Goldstein, H. 1980, *Classical Mechanics*, p. 143, (Addison-Wesley).
- Han, J. L. & Manchester, R. N. 2000, astro-ph/0010538.
- Jones, P. B. 1988, MNRAS, 235, 545.
- Jones, P. B. 1992, MNRAS, 257, 501.
- Jones, D. I. & Andersson, N. 2000, astro-ph/0011063.
- Lamb, H. 1952, *Hydrodynamics* (Cambridge University Press).

- Landau, L. & Lifshitz, E. M. 1976, *Mechanics*, pp. 110-111, (Pergamon).
- Link, B., Epstein, R. I. & Lattimer, J. M. 1999, *Phys. Rev. Lett.*, 83, 3362.
- Link, B., Franco, L. M. & Epstein, R. I. 1998, *ApJ*, 508, 838.
- Lyne, A. G., Pritchard, R. S. & Smith, F. G. 1988, *MNRAS*, 233, 667.
- Melatos, A. 2000, *MNRAS*, 313, 217.
- Mendell, G. 1998, *MNRAS*, 296, 903.
- Munk, W. & MacDonald, G. J. F. 1960, *The Rotation of the Earth* (New York: Cambridge University Press).
- Nelson, R. W., Finn, L. S. & Wasserman, I. 1990, *ApJ*, 348, 226.
- Orford, K. J. 1987, *Ap&SS*, 129, 181.
- Pines, D. & Shaham, J. 1974, *Comments on Modern Physics, Part C*, 6, 37.
- Sedrakian, A., Wasserman, I. & Cordes, J. M. 1999, *ApJ*, 524, 341.
- Shabanova, T. V., Lyne, A. G. & Urama, J. O. 2001, *astro-ph/0101282*.
- Shaham, J. 1977, *ApJ*, 214, 251.
- Shakura, N. I., Postnov, K. A. & Prokhorov, M. E. 1998, *A&A*, 331, L37.
- Stairs, I. H., Lyne, A. G. & Shemar, S. L. 2000, *Nature*, 406, 484.
- Suto, Y. & Iso, K.-I. 1985, *Ap&SS*, 115, 243.
- Tannanbaum, H., Gursky, H., Kellog, E. M., Levinson, R., Schreier, E., Giacconi, R. 1972, *ApJ*, 174, L143.
- Trümper, J., Kahabka, P., Ögelman, H., Pietsch, W., Voges, W. 1986, *ApJ*, 300, L63.
- Ushomirsky, G., Cutler, C. & Bildsten, L. 2000, *astro-ph/0001129*.
- Weisberg, J. M., Romani, R. W. & Taylor, J. H. 1989, *ApJ*, 347, 1030.

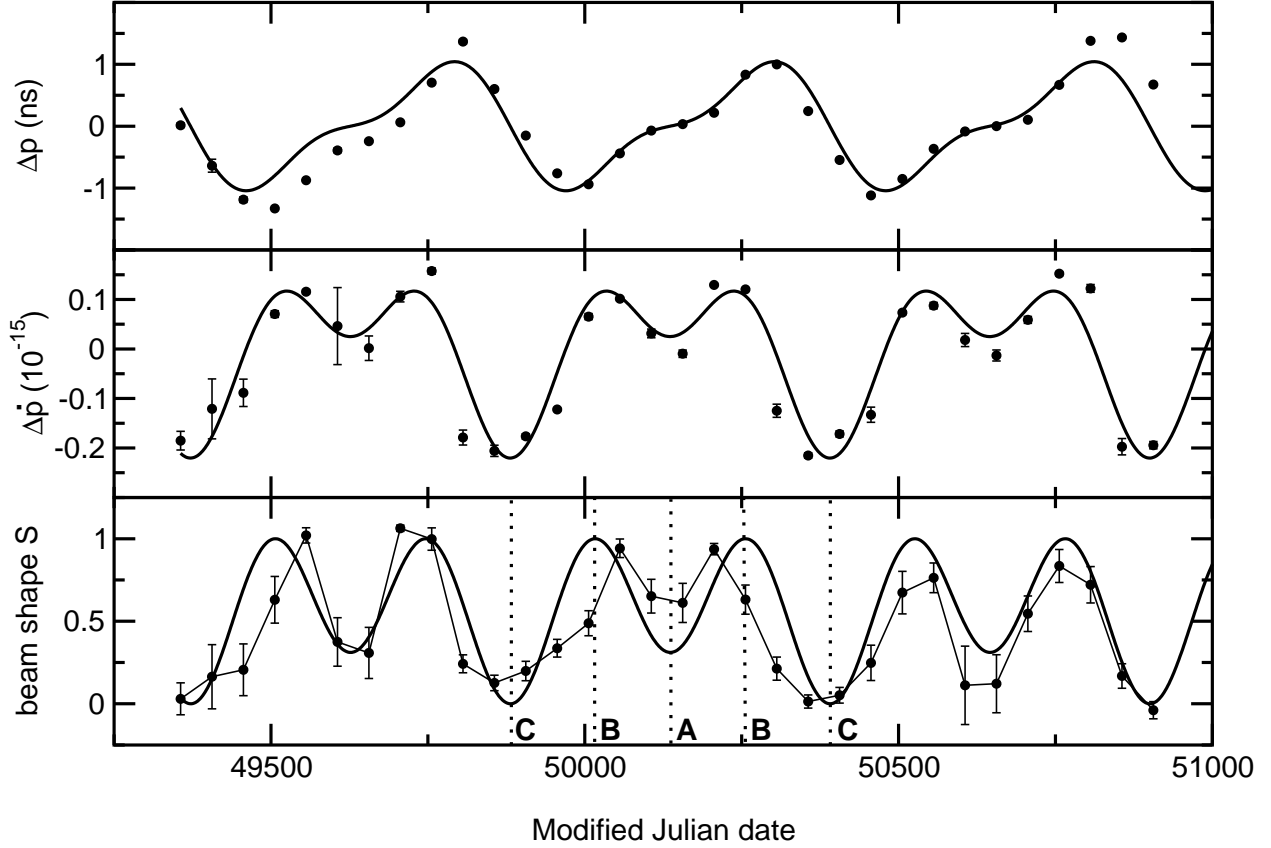


Fig. 1.— Timing and beam shape data for PSR B1828-11 (from Stairs, Lyne & Shemar 2000). Only the most-densely sampled portion of the 13-year data span is shown. The top panel gives the period residuals with respect to the star’s secular spin down. The middle panel is the time derivative. The bottom panel shows the shape parameter of Stairs, Lyne & Shemar (2000); it is $S = A_N / (A_N + A_W)$, where A_N and A_W are the fitted heights of the narrower and wider profiles, so that $S \simeq 0$ for wide pulses and $S \simeq 1$ for narrow ones. The data points give average values of S , obtained by averaging S over multiple bins. The solid curves for Δp and $\Delta \dot{p}$ are the fit described in the text. The jagged line in the lower panel is a guide to the eye.

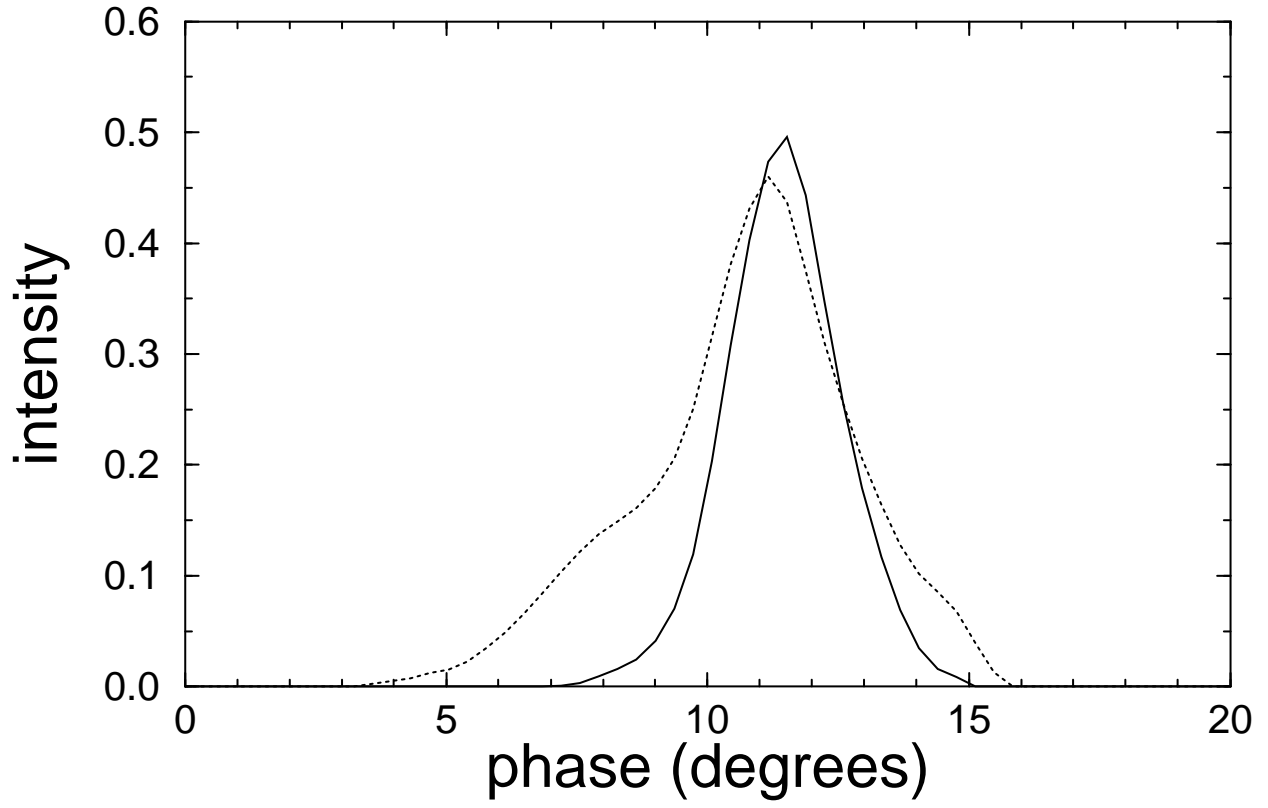


Fig. 2.— Templates for the wide and narrow beam profiles of PSR B1828-11 (courtesy I. Stairs).

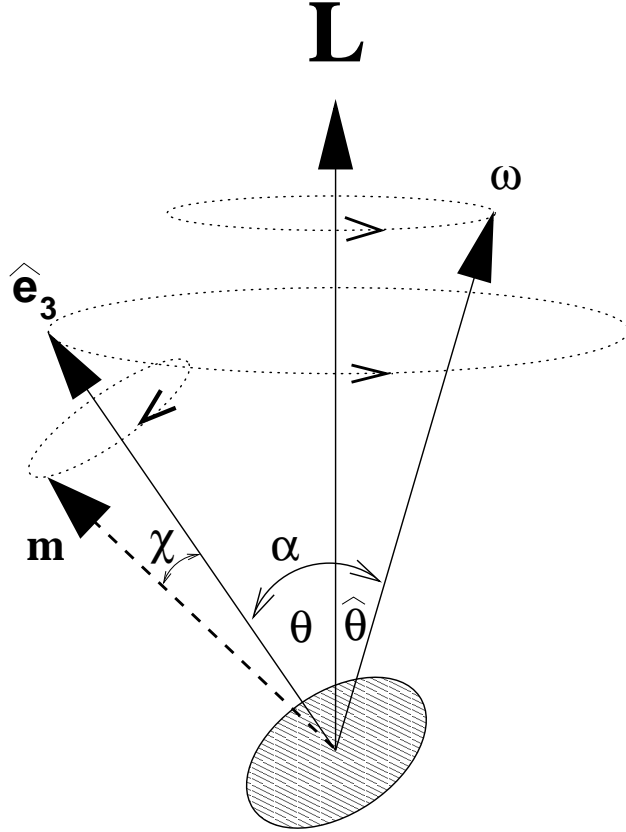


Fig. 3.— Geometry of free precession of a biaxial neutron star in the inertial frame. The body’s symmetry axis is denoted by \hat{e}_3 , the angular momentum by \mathbf{L} and the angular velocity by $\boldsymbol{\omega}$; the three vectors always span a plane as shown. The angles θ , $\hat{\theta}$ and α are constant, with $\hat{\theta} \simeq \epsilon\theta \ll \theta$ for small oblateness ϵ . The vectors \hat{e}_3 and $\boldsymbol{\omega}$ rotate about \mathbf{L} at nearly the spin frequency ω . A dipole moment \mathbf{m} fixed in the body, and taking an angle χ with respect to \hat{e}_3 , rotates in a retrograde sense about \hat{e}_3 at frequency $\simeq \epsilon\omega$.

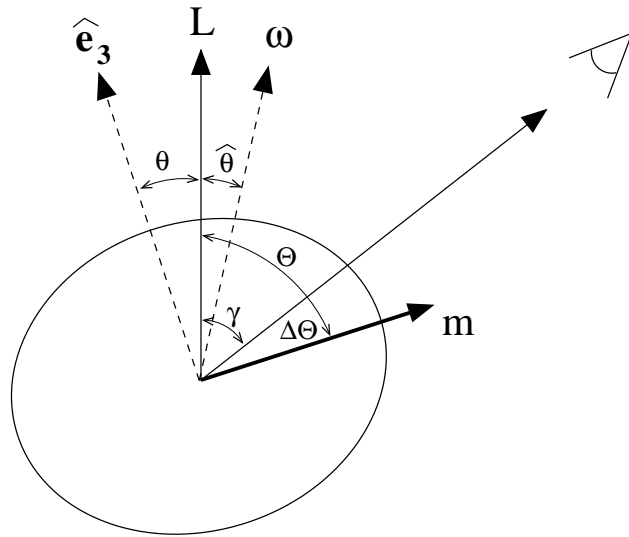


Fig. 4.— Observing geometry. At the instant the dipole moment \mathbf{m} is in the plane containing the angular momentum \mathbf{L} and the observer, the angles are defined as shown.

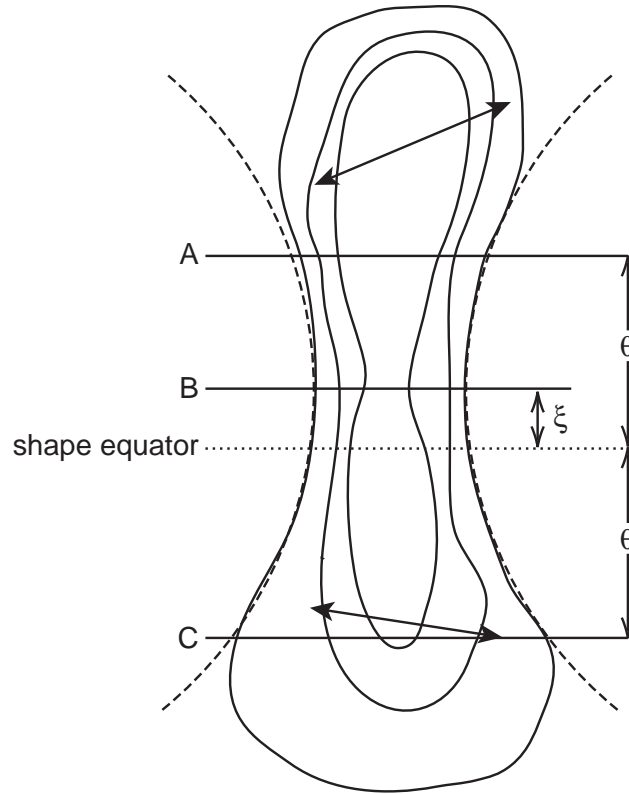


Fig. 5.— The beam pattern for the radio emission from PSR B1828-11. The dashed parabolas represent the analytic fit to the beam width, and the contour curves are one possible realization of the actual beam shape. As the star precesses, observer’s line of sight varies by $\pm\theta$ about the star’s shape equator, the dotted horizontal line. The solid lines A and C give the range of the viewing angles. Line B represents the viewing angle at which the beam is the narrowest. The double-headed arrows represent plausible polarization directions.